Chinese Journal of
POLYMER SCIENCE

RESEARCH ARTICLE

https://doi.org/10.1007/s10118-023-2916-4
Chinese J. Polym. Sci. **2023**, *41*, 1269–1276

Meniscus-Assisted Solution Printing Enables Cocrystallization in Poly(3-alkylthiophene)-based Blends for Field-Effect Transistors

Shu-Yin Zhu and Juan Peng*

State Key Laboratory of Molecular Engineering of Polymers, Department of Macromolecular Science, Fudan University, Shanghai 200438, China

Electronic Supplementary Information

Abstract The formation of cocrystallization in two various conjugated components may endow the newly formed conjugated cocrystals with multiple functionalities and improved charge transport properties. However, compared to conjugated small molecules, this strategy is rather limitedly realized in conjugated polymers. Herein, a simple meniscus-assisted solution printing (MASP) strategy is utilized to achieve the cocrystallization in the blends of two conjugated polymers, *i.e.*, poly(3-hexylthiophene) (P3HT) and poly(3-octylthiophene) (P3OT), and the cocrystalline structures are correlated closely to their charge mobilities. The P3HT/P3OT blends phase separate and crystallize individually in their drop-cast thin films. When subjecting the P3HT/P3OT blended solution to MASP, the confined solvent evaporation between two nearly parallel plates triggers them to cocrystallize progressively when accelerating the moving lower plate. The cocrystallization kinetics and the changes in P3HT/P3OT molecular structures are elucidated. Finally, these different crystalline structures of P3HT/P3OT blends are applied in organic field-effect transistors, imparting the cocrystallization-enhanced charge transport than respective P3HT and P3OT crystal domains. Such MASP method can be extended to craft cocrystals of other conjugated polymer blends for their diverse optoelectronic applications.

Keywords Conjugated polymer blends; Polythiophene; Cocrystallization; Charge mobility; Meniscus-assisted solution printing

Citation: Zhu, S. Y.; Peng, J. Meniscus-assisted solution printing enables cocrystallization in poly(3-alkylthiophene)-based blends for field-effect transistors. *Chinese J. Polym. Sci.* **2023**, *41*, 1269–1276.

INTRODUCTION

Conjugated polymers have been largely adopted in organic electronics due to their fascinating optical and electrical properties.[1–3] The key concept for conjugated polymers is their structure-property correlation. The charge transport property of conjugated polymers is primarily affected by their chemical structures with π-electrons delocalized along backbones. Basically, the more planar backbone, increased conjugation length, and narrower π-π stacking distance are favorable for the charge transport.[4,5] As a result, a number of conjugated polymers with new chemical structures have been synthesized to meet these criteria.[6–12] Likewise, the molecular packing and crystalline structures of these conjugated polymers in their solid state play a vital role in the charge transport, which can be controlled at different stages of crystallization (*i.e.*, solution-state,[13,14] film-deposition process,[15–17] and post-processing[18–20]). For example, remarkably enhanced charge mobilities are achieved in some conjugated polymers with various molecular and electronic structures by controlling the growth of nanofibrils and aligning backbones *via* natural brush-printing.[21] The design of new chemical structures and processing in their various states can be either solely, or collectively utilized to enhance the charge transport of conjugated polymers.

Usually, the semiconducting layer in most organic field-effect transistors (OFETs) contains only single material. Recently, a promising cocrystallization method has been utilized in OFETs by involving two or more materials into cocrystals, exhibiting synergistic and collective properties of different materials.[22–25] These organic cocrystals are mostly focused on conjugated small molecules produced through non-covalent interactions.[22,23] Nonetheless, very few work have been reported based on conjugated polymer cocrystals due to the difficulty in obtaining their cocrystals as three prerequisites should be met simultaneously including similar structures, close crystalline kinetics, and comparable potential energies.[24–28] Moreover, the investigation into controlling the cocrystallization kinetics is rather limited.[29]

Herein, we utilize a simple meniscus-assisted solution printing (MASP) method to efficiently achieve cocrystallization in two poly(3-alkylthiophene)s (P3HT and P3OT) , elucidate their cocrystallization kinetics and charge transport properties. During the MASP, the P3HT/P3OT blended solution was injected into two-nearly-parallel plates[29–33] with the movable lower plate controlled by a computer against the upper stationary plate. The confined solvent evaporation yielded a

* Corresponding author, E-mail: juanpeng@fudan.edu.cn
Received October 16, 2022; Accepted November 28, 2022; Published online February 7, 2023

© Chinese Chemical Society
Institute of Chemistry, Chinese Academy of Sciences

meniscus at the edge of the two plates, carried the P3HT and P3OT to the solution edge, and assisted the film formation after drying. Intriguingly, the P3HT/P3OT blends self-assembled into cocrystals progressively when accelerating the moving lower plate. This yielded an improved charge mobility (μ) for the cocrystal film of P3HT/P3OT compared to their respective components and drop-cast phase-separated structures, demonstrating the cocrystal film is favorable for the charge transport. This MASP strategy is extremely simple and efficient, and can be easily applied to other conjugated blends for the production of cocrystallization.

EXPERIMENTAL

Materials

Five monomers, 2-bromo-5-iodo-3-butylthiophene, 2-bromo-5-iodo-3-hexylthiophene, 2-bromo-5-iodo-3-octylthiophene, 2-bromo-5-iodo-3-decylthiophene and 2-bromo-5-iodo-3-dodecylthiophene were synthesized based on the reported approach.[34] Isopropylmagnesium chloride (*i*-PrMgCl, 2.0 mol/L in tetrahydrofuran) and [1,3-bis(diphenylphosphino)propane]-dichloronickel(II) (Ni(dppp)Cl_2) were brought from Sigma-Aldrich. Poly(3-hexylthiophene) (P3HT, M_n=14.3K, PDI=1.09) and poly(3-octylthiophene) (P3OT, M_n=12.8K, PDI=1.10) were synthesized *via* Kumada catalyst-transfer polymerization (KCTP) (Figs. S1 and S2 and Table S1 in the electronic supplementary information, ESI).[35,36] For comparison, poly(3-butylthiophene) (P3BT, M_n=12.5K, PDI=1.12), poly(3-decylthiophene) (P3DT, M_n=12.4K, PDI=1.11), and poly(3-dodecylthiophene) (P3DDT, M_n=11.6K, PDI=1.10) were synthesized as well (Figs. S1 and S2 and Table S1 in ESI).

Formation of P3HT/P3OT Blended Films *via* Meniscus-assisted Solution Printing (MASP)

The P3HT/P3OT blended solution (10 mg/mL, ~20 μL) was loaded within two plates[29–33] at an angle of ~10° and a separation distance (H) of ~150 μm. The lower plate (Si substrate) was mounted on a motorized movable stage with the moving speeds in the range of 5–80 μm/s controlled by a computer, while the upper plate (glass slide) was fixed (Parker Hannifin Corp). During the MASP process, the evaporating solvents transported the chains of polymer blends to the menicus edge, triggered them to dry and deposit into a continuous film over a large area.

Fabrication Procedures for Organic Field-Effect Transistors (OFETs)

Top-contact, bottom-gate OFETs were prepared on highly n-doped silicon wafers with a layer of SiO_2 (~300 nm). After drop-casting or MASP process to obtain the blended films, a gold layer (thickness: ~30 nm) was evaporated onto the blended film as the source/drain electrodes (channel length: 30 μm, channel width: 300 μm).

Characterization

^{1}H-NMR were performed on a DMX 500 MHz spectrometer using tetramethylsilane (TMS) as the internal standard in $CDCl_3$. Gel permeation chromatography (GPC) was carried out on an Agilent 1260 system (eluent: THF). Two-dimensional grazing-incidence wide angle X-ray scattering (2D-GIWAXS) experiments were performed at the Shanghai Synchrotron Radiation Facility (SSRF) (beamline: BL14B1, wavelength: 1.24 Å). X-ray diffraction (XRD) spectra were obtained on a PANalytical X'Pert PRO X-ray diffractometer using Cu Kα radiation (wavelength: 1.541 Å) operating at 40 kV and 40 mA. Differential scanning calorimetry (DSC) was carried out using a Q2000 calorimeter (TA Instruments). UV-Vis absorption spectra were collected on a PerkinElmer Lambda 750 UV-Vis spectrophotometer. Atomic force microscopy (AFM) was carried out on the Bruker Fast Scan system. The OFET characteristics were obtained with a Keithley 4200-SCS parameter analyzer in an argon-filled glovebox.

RESULTS AND DISCUSSION

Fig. 1(a) schematically shows the setup for MASP, with the confinement of the P3HT/P3OT blended toluene solution. The bottom plate could be moved by controlling a computer against the upper stationary plate. During MASP, the P3HT and P3OT chains can be continuously transported to the meniscus edge and deposit into a complete film over a large scale. A side-view of MASP is given in the inset of Fig. 1(a), depicting the constrained P3HT/P3OT blended solution within the two close plates with a concave meniscus.

To explore the changes in the molecular packing and crystalline structures of P3HT/P3OT blended films upon MASP, 2D-GIWAXS was performed, with the schematic described in Fig. 1(b). For a thorough comparison, the drop-cast P3HT and P3OT homopolymers were also investigated. P3HT and P3OT exhibit their respective (100) diffractions in the out-of-plane direction at q_z=4.00 and 3.25 nm^{-1}, corresponding to the d_{100} values of 1.57 and 1.93 nm, respectively (Fig. S3 in ESI). Their (010) diffractions are at $q_{x,y}$=16.6 nm^{-1} (d_{010}=0.38 nm) in the in-plane direction. It indicated the two polymers packed into an edge-on orientation in which the alkyl side chain direction and π-π stacking direction are oriented normal and parallel to the substrate, respectively. For a more detail analysis, the (100) diffraction peak of P3OT has a narrower full width at half maximum (FWHM$_{100}$=0.52 nm^{-1}) than that of P3HT (FWHM$_{100}$=0.59 nm^{-1}), implying a higher crystal ordering in the former.

For the P3HT/P3OT blended film without MASP, it displays two (100) peaks at q_z of 3.86 (d_{100}=1.63 nm) and 3.34 nm^{-1} (d_{100}=1.88 nm) for the drop-cast film, attributed to the P3HT and P3OT crystal domains, respectively (Figs. 1c and 1e). It evidenced that the phase separation occurred in the drop-cast P3HT/P3OT blends. In contrast, the P3HT/P3OT blended solution during MASP at the moving speed (v) of 20 μm/s displays single (100) diffraction peak (q_z=3.52 nm^{-1}, d_{100}=1.78 nm) (Figs. 1d and 1e). The d_{100} spacing is between that of P3HT and P3OT homopolymers, indicative of the formation of cocrystallization in the edge-on manner. The FWHM$_{100}$ of the P3HT/P3OT cocrystal is 0.92 nm^{-1}, which is broader than that of respective homopolymer, indicating a less ordered crystalline structure in the cocrystals. The P3HT/P3OT blended samples before (*i.e.*, their drop-cast film) and after MASP (v=20 μm/s) were further characterized by DSC. The drop-cast P3HT/P3OT blends exhibit two peaks at 188 and 230 °C, which attribute to the melting point of P3OT and P3HT, respectively (Fig. S4 in ESI). While the P3HT/P3OT blends upon MASP at v=20 μm/s only show one single peak at 207 °C,

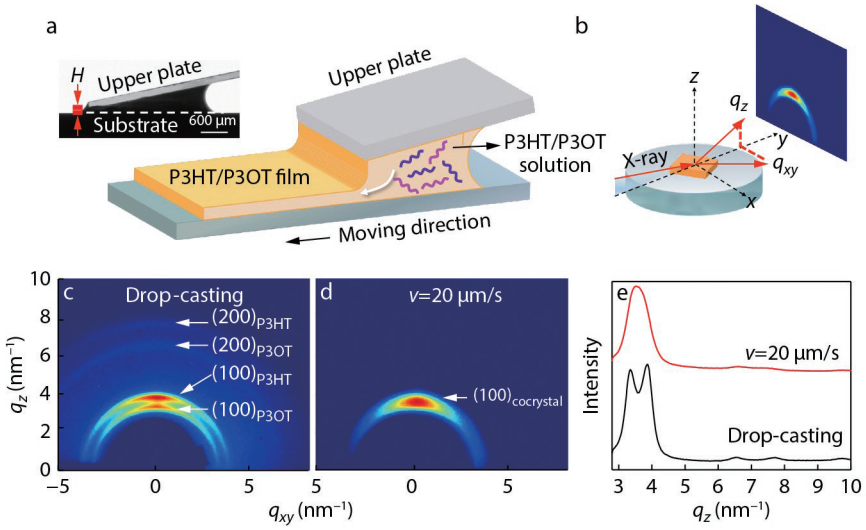

Fig. 1 (a) Schematic representation of the production of P3HT/P3OT cocrystals *via* meniscus-assisted solution printing (MASP). The P3HT/P3OT blended solution is constrained within two close plates. The lower plate can be dragged while keeping the upper plate fixed, yielding the formation of P3HT/P3OT cocrystal film over a large scale after the complete solvent evaporation. The inset is the device side-view photograph. (b) Schematic representation of the synchrotron 2D-GIWAXS experiment on the P3HT/P3OT blends. (c, d) 2D-GIWAXS and (e) the corresponding 1D-GIWAXS patterns of (c) P3HT/P3OT blended film drop-cast from toluene and (d) P3HT/P3OT blended film after MASP at *v*=20 μm/s.

ascribed to the melting point of their cocrystals (Fig. S4 in ESI). These DSC results agreed well with the GIWAXS data, further proving the phase separation and separated crystallization in drop-cast P3HT/P3OT blends while the formation of cocrystals after MASP.

In what follows, the cocrystallization kinetics of the P3HT/P3OT blended solution during MASP were elucidated. To track the cocrystallization kinetics more clearly, a mixed solvent of chloroform/dichlorobenzene ($CHCl_3$/ODCB, 7/3, *V*/*V*) was used, which could slow down the solvent evaporation greatly but did not change their phase-separated structure in the initial drop-cast film (Fig. 2a). At a low *v* of 5 μm/s, P3HT/P3OT blended sample displays two distinct (100) diffraction peaks, not much different from their drop-cast sample (Fig. 2b). By increasing *v* from 10 μm/s, 20 μm/s to 50 μm/s, the arcs of the two (100) diffractions still exist (Figs. 2c–2e). However, their 1D-GIWAXS patterns clearly show the two (100) peaks gradually approached to each other (Fig. 2g), implying the ongoing cocrystallization process between P3HT and P3OT. Finally, these two (100) peaks merge into one single (100) peak at *v*=80 μm/s, as observed from both 2D and 1D-GIWAXS patterns (Figs. 2f and 2g), indicating the formation of cocrystals between P3HT and P3OT chains at this speed. When the solvent was changed from toluene to mixture of $CHCl_3$/ODCB, the mixed solvents evaporated much slower than toluene. Therefore, the P3HT/P3OT blends needed stronger driving force to render them to cocrystallize. As a result, a higher *v* (*i.e.*, 80 μm/s) was needed to obtain the P3HT/P3OT cocrystals. The changes of the d_{100} values of P3HT and P3OT and their d_{100} difference (Δd_{100}) during MASP are depicted in Fig. 2(h). Clearly, the d_{100} of P3HT and P3OT in the blends gradually got closer with the increased *v*, and finally achieved to their difference of 0 (Δd_{100}=0) in the cocrystal film.

Subsequently, the microstructure and quality of the P3HT/P3OT blended films prepared during MASP were imaged by AFM (Fig. 3). All the P3HT/P3OT films show no apparent topographical features, and the blended films displayed smaller microdomains with the increased *v*. During the MASP to form the P3HT/P3OT film, the homopolymer with lower surface energy is more energetically favorable to enrich at the polymer-air interface. Due to the lower surface energy of P3OT than P3HT, most P3OT may locate at the polymer-air interface and thus display featureless topography although the P3HT/P3OT structures changed from phase separation to cocrystals. The blended films displayed a decreased root-mean-square (RMS) roughness from drop-cast 19.7 nm to 4.52 nm (*v*=80 μm/s). It indicated the P3HT/P3OT cocrystal film had a smoother surface than its phase-separated film. With the increased MASP speed, the speeded-up solvent evaporation produced more crystal nucleus with smaller size, leading to the decreased RMS roughness.

From the above results, it is clear that the MASP efficiently transformed the phase-separated P3HT/P3OT blends in their drop-cast state into cocrystals. Although P3HT and P3OT have similar chemical structures, their different side-chain lengths endow them with different crystallization rates.[37] Before MASP, the natural solvent evaporation rendered P3HT and P3OT enough time to phase separate and thus crystallize separately. When subjecting the P3HT/P3OT blended solution to MASP, the solvent evaporation is speeded up with the increased moving speed of the lower plate. As a result, P3HT and P3OT gradually have no enough time to phase separate, leading to their cocrystallization. A schematic representation of the cocrystallization in P3HT/P3OT blends during MASP is depicted in Fig. 4. From the viewpoint of molecular packing, both P3HT and P3OT chains were coil-like in the solution. The solvent evaporation enabled by MASP gradually changed their conformation from coil-like to rod-like. Subsequently, these rod-like P3HT and P3OT chains interact with each other to *π*-*π* stack into cocrystals in the film state with their hexyl and octyl side chains packed into end-to-end mode, yielding

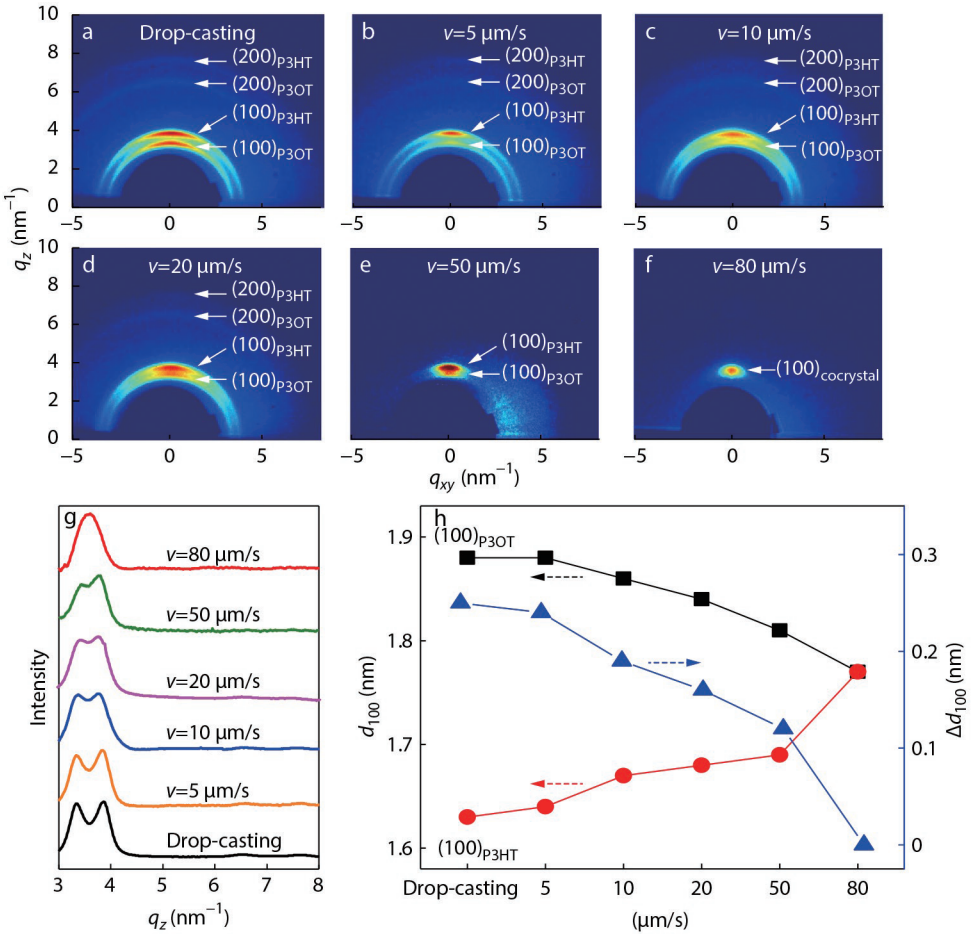

Fig. 2 (a–f) 2D-GIWAXS and (g) the corresponding 1D-GIWAXS patterns of P3HT/P3OT blended films (a) when drop-casting from $CHCl_3$/ODCB mixed solvents and (b–f) after MASP at *v* of (b) 5, (c) 10, (d) 20, (e) 50, and (f) 80 μm/s, respectively. (h) The histograms summarizing the changes of the interlayer spacing (d_{100}) of P3HT and P3OT and their interlayer spacing difference (Δd_{100}) during MASP.

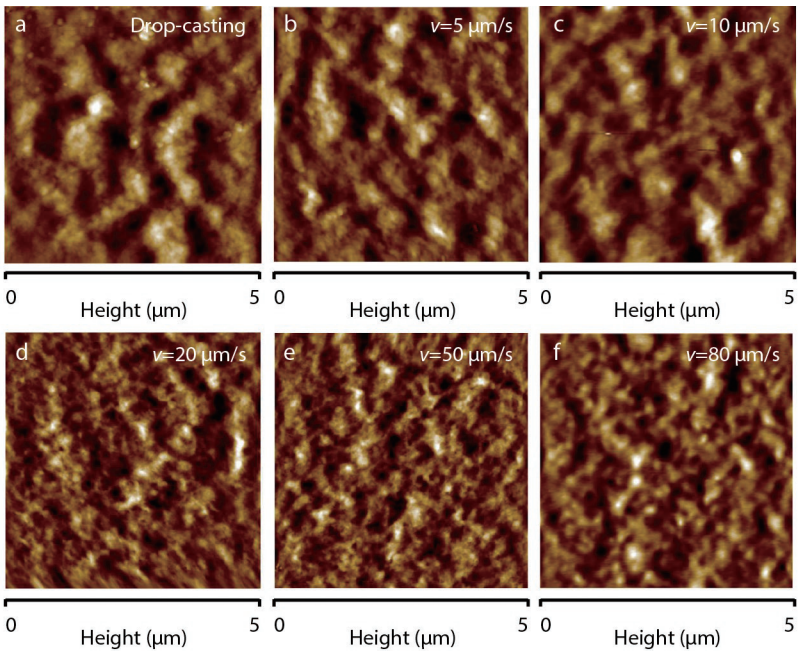

Fig. 3 (a–f) AFM height images of (a) P3HT/P3OT blended film drop-cast from $CHCl_3$/ODCB mixed solvents and (b–f) P3HT/P3OT blended films after MASP at *v* of (b) 5, (c) 10, (d) 20, (e) 50, and (f) 80 μm/s, respectively.

https://doi.org/10.1007/s10118-023-2916-4

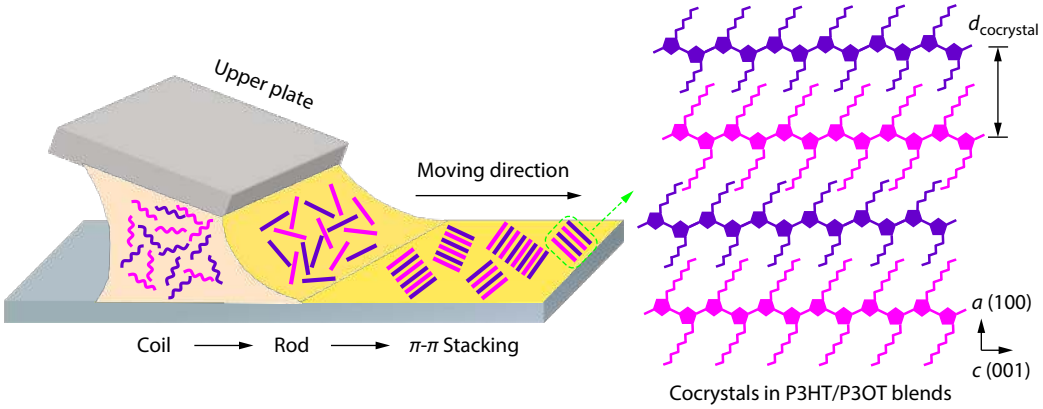

Fig. 4 Schematic illustration of the cocrystallization in P3HT/P3OT blends during MASP. During the solvent evaporation enabled by MASP, both chains of P3HT and P3OT occurred coil-to-rod changes, followed by the *π*-*π* stacking mutually to cocrystallize. The side hexyl and octyl chains interdigitated along the (100) direction to produce a balanced d_{100}-spacing. *a*- and *c*-axes represent the alkyl packing (100) direction and thiophene backbone (001) direction, respectively.

a balanced d_{100}-spacing.

We note that the key to the success in the cocrystallization of P3HT/P3OT blends is their suitable difference between two alkyl side chains. For comparison, poly(3-alkylthiophene)/poly(3-alkylthiophene) (P3AT/P3AT) blends with larger side chain differences were subjected to MASP as well, including P3BT/P3OT, P3HT/P3DT, P3BT/P3DT, P3HT/PDDT, and P3BT/P3DDT with their side chain differences of four (*i.e.*, P3BT/P3OT and P3HT/P3DT), six (*i.e.*, P3BT/P3DT and P3HT/PDDT), and eight (P3BT/P3DDT) carbon atoms. As characterized by XRD, in all five pairs of P3AT/P3AT blends, they exhibited respective (100) diffraction peaks in the drop-cast state (Fig. S5a in ESI). After subjecting their blended solution to MASP at *v* of 20 and 80 μm/s, all of them remained individual crystal domains instead of cocrystallization (Figs. S5b and S5c in ESI). Since the differences in the side chain length of five P3AT/P3AT blends are larger than that of P3HT/P3OT blends, their crystallization kinetics are more different than that of P3HT/P3OT. Therefore, these five P3AT/P3AT blends have stronger tendency to crystallize individually than P3HT/P3OT. This yielded their phase-separated structures instead of cocrystals upon MASP. Interestingly, a recent work demonstrated that the cocrystals could be realized in the poly(2,5-bis(3-hexylthiophen-2-yl)thieno[3,2-*b*]thiophene) (PBTTT-C6) and poly(2,5-bis(3-decylthiophen-2-yl)thieno[3,2-*b*]thiophene) (PBTTT-C10) blends upon MASP.[29] These PBTTT blends had similar hair-rod configuration to P3ATs but larger side chain difference (*i.e.*, four carbon atoms). It suggests that it may be easier to achieve cocrystallization in PBTTT blends than in P3AT blends.

To explore the optical properties of various P3HT/P3OT samples, their UV-Vis measurements were performed (Fig. 5). The drop-cast P3HT/P3OT blended film shows three absorption peaks at 520, 550 and 600 nm. The peaks at 520 and 550 nm are ascribed to the *π* to π^* transition of polythiophene intrachain.[38] The absorption vibronic peak at 600 nm is ascribed to the interchain *π*-*π* interaction. Upon MASP with the increased *v*, it can be seen that the peak around 520 nm gradually decreased, implying progressively weakened intrachain interaction. In contrast, the vibronic peak at 600 nm gradually increased, among which the P3HT/P3OT blended

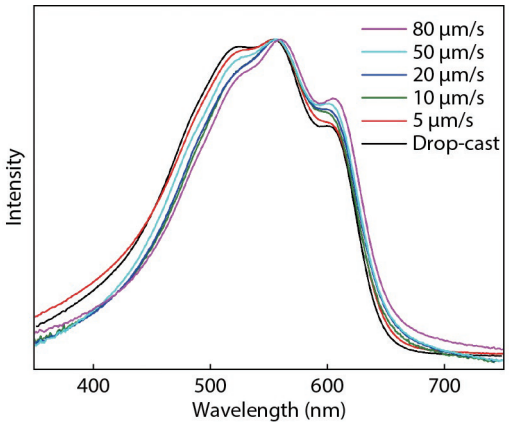

Fig. 5 Normalized UV-Vis absorption spectra of the P3HT/P3OT blended films drop-cast from $CHCl_3$/ODCB mixed solvents and after MASP at various *v*.

sample at *v*=80 μm/s displayed the strongest vibronic peak. It implied that the interchain *π*-*π* interaction in P3HT/P3OT systems was strengthened with the increased *v*. In conjunction with the GIWAXS results that the cocrystals between P3HT and P3OT chains were rendered at *v*=80 μm/s, it indicated the P3HT/P3OT cocrystals had the strongest *π*-*π* interaction.

To investigate the device performance of the phase-separated and cocrystalline structures in P3HT/P3OT blends, OFETs in bottom-gate, top-contact structure were crafted (Fig. 6, Fig S6 in ESI and Table 1). The drop-cast P3HT/P3OT films show an average *μ* of 1.61×10^{-4} $cm^2\cdot V^{-1}\cdot s^{-1}$. After MASP with the increased *v* (5–80 μm/s), the P3HT/P3OT blends display gradually increased average *μ* from 1.07×10^{-3} $cm^2\cdot V^{-1}\cdot s^{-1}$ to 4.69×10^{-3} $cm^2\cdot V^{-1}\cdot s^{-1}$. The P3HT/P3OT blended film at *v*=80 μm/s showed the highest *μ* of 4.97×10^{-3} $cm^2\cdot V^{-1}\cdot s^{-1}$. Since the GIWAXS results revealed the tendency to cocrystallize in P3HT/P3OT blends during MASP and they reached the cocrystallization at *v*=80 μm/s, it signified that the P3HT/P3OT cocrystal films were more favorable to the charge transport than their respective crystal domains. It is reasonable that charges transport faster in a uniform crystal domain than different crystal domains due to the crystalline boundary in the latter. For comparison, respective P3HT and P3OT solutions

https://doi.org/10.1007/s10118-023-2916-4

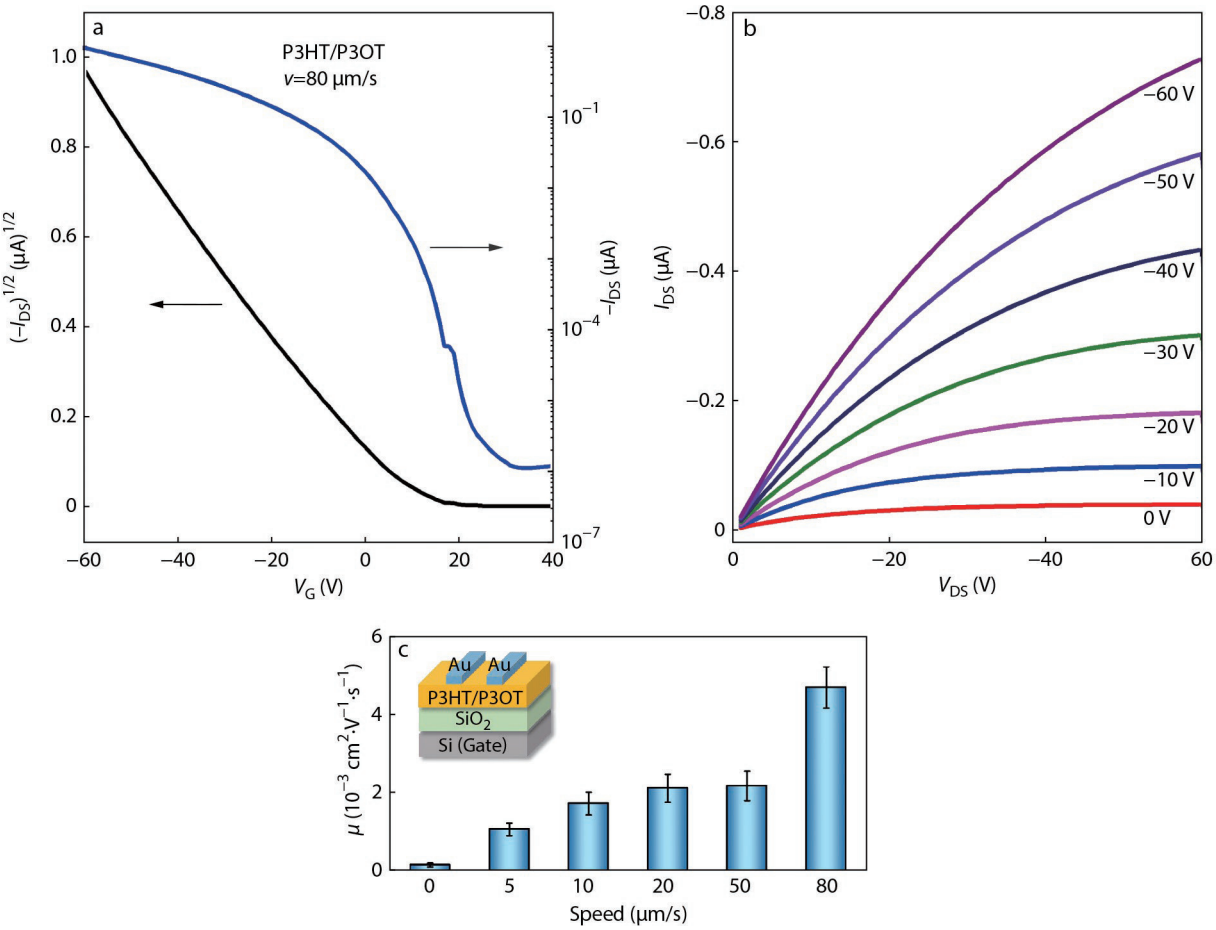

Fig. 6 (a) OFET transfer and (b) output characteristics of the P3HT/P3OT cocrystalline film achieved after MASP at v=80 μm/s, V_{DS}=−60 V; (c) Summary of OFET results of the P3HT/P3OT blended films drop-cast from $CHCl_3$/ODCB mixed solvents (*i.e.*, v=0 μm/s) and after MASP at various v. The schematic of the OFET device is described in the inset of (c).

Table 1 Summary of OFET performance of P3HT/P3OT blended films under various conditions.

Samples	μ_{max} [a] ($cm^2 \cdot V^{-1} \cdot s^{-1}$)	μ_{avg} [b] ($cm^2 \cdot V^{-1} \cdot s^{-1}$)	I_{on}/I_{off} [c]	V_{th} [d] (V)
Drop-casting	2.81×10^{-4}	1.61×10^{-4}	5–10	>60
5 μm/s	1.30×10^{-3}	1.07×10^{-3}	10^2–10^4	14–20
10 μm/s	1.95×10^{-3}	1.73×10^{-3}	10^2–10^4	6–10
20 μm/s	2.35×10^{-3}	2.12×10^{-3}	10^3–10^6	12–15
50 μm/s	2.48×10^{-3}	2.18×10^{-3}	10^3–10^5	6–14
80 μm/s	4.97×10^{-3}	4.69×10^{-3}	10^3–10^6	4–16

[a] Maximum charge mobility; [b] Average charge mobility; [c] Current on/off ratio; [d] Threshold voltage.

were also subjected to MASP at v=80 μm/s. Their films showed the average charge mobilities of 1.44×10^{-3} $cm^2 \cdot V^{-1} \cdot s^{-1}$ for P3HT and 6.66×10^{-4} $cm^2 \cdot V^{-1} \cdot s^{-1}$ for P3OT (Fig. S7 in ESI), respectively, which were lower than that of the P3HT/P3OT at v=80 μm/s. This result further underpined the cocrystal-facilitated charge transport since P3HT with shorter side chains can improve the film crystallinity and P3OT with longer side chains can improve the solubility in the solution.

CONCLUSIONS

In summary, we attained the cocrystallization over respective crystallization in P3HT/P3OT conjugated polymer blends *via* an efficient MASP strategy and connected their different crystalline structures to charge transport properties. Specifically, the drop-cast P3HT/P3OT blends phase-separated and formed individual P3HT and P3OT crystal domains. Upon MASP with the increased speed, the P3HT/P3OT blends gradually transformed into cocrystallization with two various alkyl chains packed in an end-to-end mode along the mutual alkyl stacking direction. The MASP accelerated the solvent evaporation and thus rendered the cocrystallization of P3HT and P3OT since they did not have enough time to phase separate from each other. Importantly, the P3HT/P3OT cocrystals exhibited a higher average μ than their phase-separated films and respective homopolymer films. It indicated a superior charge transport in P3HT/P3OT cocrystal film. Overall, this work demonstrated the robustness of MASP in the production of polythiophene-based cocrystals and provided

https://doi.org/10.1007/s10118-023-2916-4

insights into the solution processing-cocrystallization-charge transport property correlation, which may underpin their application in various optoelectronic devices.

Conflict of Interests

The authors declare no interest conflict.

Electronic Supplementary Information

Electronic supplementary information (ESI) is available free of charge in the online version of this article at http://doi.org/10.1007/s10118-023-2916-4.

ACKNOWLEDGMENTS

This work was financially supported by the National Natural Science Foundation of China (Nos. 21922503 and 22173023) and Natural Science Foundation of Shanghai (No. 21ZR1405800). We gratefully acknowledge the support from Shanghai Synchrotron Radiation Facility of China for using the BL14B1 beamline.

REFERENCES

1 Li, Q. Y.; Lei, T.; Yao, Z. F.; Wang, J. Y.; Pei, J. Multi-level self-assembly of conjugated polymers. *Acta Polymerica Sinica* (in Chinese) **2019**, *50*, 1–12.
2 Zhao, Y.; Guo, Y. L.; Liu, Y. Q. 25th Anniversary article: recent advances in n-type and ambipolar organic field-effect transistors. *Adv. Mater.* **2013**, *25*, 5372–5391.
3 Yin, Y.; Zhai, D. L.; Chen, S. W.; Shang, X.; Li, L. X.; Peng, J. Controlling the condensed structure of polythiophene and polyselenophene-based all-conjugated block copolymers. *Acta Polymerica Sinica* (in Chinese) **2020**, *5*, 434–447.
4 Mei, J.; Diao, Y.; Appleton, A. L.; Fang, L.; Bao, Z. Integrated materials design of organic semiconductors for field-effect transistors. *J. Am. Chem. Soc.* **2013**, *135*, 6724–6746.
5 McCullough, R. D. The chemistry of conducting polythiophenes. *Adv. Mater.* **1998**, *10*, 93–116.
6 Ding, J.; Liu, Z.; Zhao, W.; Jin, W.; Xiang, L.; Wang, Z.; Zeng, Y.; Zou, Y.; Zhang, F.; Yi, Y.; Diao, Y.; McNeill, C. R.; Di, C. A.; Zhang, D. Q.; Zhu, D. B. Selenium-substituted diketopyrrolopyrrole polymer for high-performance p-type organic thermoelectric materials. *Angew. Chem.* **2019**, *131*, 19170–19175.
7 Yang, C. Y.; Jin, W. L.; Wang, J.; Ding, Y. F.; Nong, S. Y.; Shi, K.; Lu, Y.; Dai, Y. Z.; Zhuang, F. D.; Lei, T.; Di, C. A.; Zhu, D. B.; Wang, J. Y.; Pei, J. Enhancing the n-type conductivity and thermoelectric performance of donor–acceptor copolymers through donor engineering. *Adv. Mater.* **2018**, *30*, 1802850.
8 Yang, J.; Xiao, B.; Heo, S. W.; Tajima, K.; Chen, F.; Zhou E. Effects of inserting thiophene as a π-bridge on the properties of naphthalene diimide-alt-fused thiophene copolymers. *ACS Appl. Mater. Interfaces* **2017**, *9*, 44070–44078.
9 Osaka, I.; Saito, M.; Mori, H.; Koganezawa, T.; Takimiya, K. Drastic change of molecular orientation in a thiazolothiazole copolymer by molecular-weight control and blending with PC61BM leads to high efficiencies in solar cells. *Adv. Mater.* **2012**, *24*, 425–430.
10 Yang, J.; Chen, J.; Sun, Y.; Shi, L.; Guo, Y.; Wang, S.; Liu, Y. Design and synthesis of novel conjugated polymers for applications in organic field-effect transistors. *Acta Polymerica Sinica* (in Chinese) **2017**, *7*, 1082-1096.
11 Jang, S.; Kim, I.; Kim, J.; Khim, D.; Jung, E.; Kang, B.; Lim, B.; Kim, Y.; Jang, Y.; Cho, K.; Kim, D. New donor-donor type copolymers with rigid and coplanar structures for high-mobility organic field-effect transistors. *Chem. Mater.* **2014**, *26*, 6907–6910.
12 Chen, Z.; Zhang, W.; Huang, J.; Gao, D.; Wei, C.; Lin, Z.; Wang, L.; Yu, G. Fluorinated dithienylethene-naphthalenediimide copolymers for high mobility n-channel field-effect transistors. *Macromolecules* **2017**, *50*, 6098–6107.
13 Yao, Z.; Wang, Z.; Wu, H.; Lu, Y.; Li, Q.; Zou, L.; Wang, J.; Pei, J. Ordered solid-state microstructures of conjugated polymers arising from solution-state aggregation. *Angew. Chem. Int. Ed.* **2020**, *59*, 17467–17471.
14 Pan, S.; Zhu, M. J.; He, L. Z.; Zhang, H. D.; Qiu, F.; Lin, Z. Q.; Peng, J. Transformation from nanofibers to nanoribbons in poly(3-hexylthiophene) solution by adding alkylthiols. *Macromol. Rapid Commun.* **2018**, *39*, 1800048.
15 Chen, S. W.; Zhu, S. Y.; Lin, Z. Q.; Peng, J. Transforming polymorphs via meniscus-assisted solution-shearing conjugated polymers for organic field-effect transistors. *ACS Nano* **2022**, *16*, 11194–11203.
16 Kyaw, A. K. K.; Lay, L. S.; Peng, G. W.; Changyun, J.; Jie, Z. A nanogroove-guided slot-die coating technique for highly ordered polymer films and high-mobility transistors. *Chem. Commun.* **2016**, *52*, 358–361.
17 Nam, S.; Jang, J.; Anthony, J. E.; Park, J. J.; Park, C. E.; Kim, K. High-performance triethylsilylethynyl anthradithiophene transistors prepared without solvent vapor annealing: the effects of self-assembly during dip-coating. *ACS Appl. Mater. Interfaces* **2013**, *5*, 2146–2154.
18 Wang, X.; Yuan, Y.; Han, L.; Dong, X.; Zhang, J. Effect of solvent annealing temperature on crystal modifications and phase transition behavior of regioregular poly(3-octylthiophene). *Chinese J. Polym. Sci.* **2014**, *32*, 1158–1166.
19 Untilova, V.; Nübling, F.; Biniek, L.; Sommer, M.; Brinkmann. M. Impact of competing crystallization processes on the structure of all-conjugated donor-acceptor block copolymers P3HT-*b*-PNDIT2 in highly oriented thin films. *ACS Appl. Mater. Interfaces* **2019**, *1*, 1660–1671.
20 Yin, Y.; Chen, S.; Zhu, S.; Li, L.; Zhai, D.; Huang, D.; Peng, J. Tailoring cocrystallization and microphase separation in rod-rod block copolymers for field-effect transistors. *Macromolecules* **2021**, *54*, 4571–4581.
21 Wang, G.; Huang, W.; Eastham, N. D.; Fabiano, S.; Manley, E. F.; Zeng, L.; Wang, B.; Zhang, X.; Chen, Z.; Li, R.; Chang, R. P. H.; Chen, L.; Bedzyk, M. J.; Melkonyana, F. S.; Facchetti, A.; Marks, T. J. Aggregation control in natural brush-printed conjugated polymer films and implications for enhancing charge transport. *Proc. Natl. Acad. Sci. U. S. A.* **2017**, *114*, E10066.
22 Park, S. K.; Varghese, S.; Kim, J. H.; Yoon, S. J.; Kwon, O. K.; An, B. K.; Gierschner, J.; Park, S. Y. Tailor-made highly luminescent and ambipolar transporting organic mixed stacked charge-transfer crystals: an isometric donor-acceptor approach. *J. Am. Chem. Soc.* **2013**, *135*, 4757–4764.
23 Zhu, W.; Zheng, R.; Fu, X.; Fu, H.; Shi, Q.; Zhen, Y.; Dong, H.; Hu, W. Revealing the charge-transfer interactions in self-assembled organic cocrystals: two-dimensional photonic applications. *Angew. Chem. Int. Ed.* **2015**, *54*, 6785–6789.
24 Zhu, M.; Pan, S.; Wang, Y.; Tang, P.; Qiu, F.; Lin, Z.; Peng, J. Unravelling the correlation between charge mobility and cocrystallization in rod-rod block copolymers for high performance field-effect transistors. *Angew. Chem. Int. Ed.* **2018**, *57*, 8644–8648.
25 Pal, S.; Nandi, A. K. Cocrystallization mechanism of poly(3-alkyl thiophenes) with different alkyl chain length. *Polymer* **2005**, *46*,

8321–8330.
26 Ge, J.; He, M.; Yang, Y.; Qiu, F. Synthesis, cocrystallization, and microphase separation of all-conjugated diblock copoly(3-alkylthiophene)s. *Macromolecules* **2010**, *43*, 6422–6428.
27 Lee, Y. H; Chen, W. C; Yang, Y. L; Chiang, C. J; Yokozawa, T.; Dai, C, A. Co-crystallization phase transformations in all π-conjugated block copolymers with different main-chain moieties. *Nanoscale* **2014**, *6*, 5208–5216.
28 Kynaston, E. L.; Winchell, K. J.; Yee, P. Y.; Manion, J. G.; Hendsbee, A. D.; Li, Y.; Huettner, S.; Tolbert, S. H.; Seferos, D. S. Poly(3-alkylthiophene)-*block*-poly(3-alkylselenophene)s: conjugated diblock co-polymers with atypical self-assembly behavior. *ACS Appl. Mater. Interfaces* **2019**, *11*, 7174–7183.
29 Zhao, Q.; Zhu, S.; Peng, J. Unraveling the co-crystallization-charge transport relation in conjugated polymer blends *via* meniscus-assisted solution-shearing. *Macromol. Rapid Commun.* **2023**, *44*, 2200622.
30 Schott, S.; Gann, E.; Thomsen, L.; Jung, S. H.; Lee, J. K.; McNeill, C. R.; Sirringhaus, H. Charge-transport anisotropy in a uniaxially aligned diketopyrrolopyrrole-based copolymer. *Adv. Mater.* **2015**, *27*, 7356–7364.
31 Yin, Y.; Zhu, S.; Chen, S.; Lin, Z.; Peng, J. Rapid meniscus-assisted solution-printing of conjugated block copolymers for field-effect transistors. *Adv. Funct. Mater.* **2022**, *32*, 2110824.
32 Giri, G.; Verploegen, E.; Mannsfeld, S. C.; Atahan-Evrenk, S.; Kim, D. H.; Lee, S. Y.; Becerril, H. A.; Aspuru-Guzik, A.; Toney, M. F.; Bao, Z. Tuning charge transport in solution-sheared organic semiconductors using lattice strain. *Nature* **2011**, *480*, 504–508.
33 He, M.; Li, B.; Cui, X.; Jiang, B.; He, Y.; Chen, Y.; O'Neil D.; Szymanski, P.; El-Sayed, M. A.; Huang, J.; Lin, Z. Meniscus-assisted solution printing of large grained perovskite films for high-efficiency solar cells. *Nat. Commun.* **2017**, *8*, 16045.
34 Yokoyama, A.; Miyakoshi, R.; Yokozawa, T. Chain-growth polymerization for poly(3-hexylthiophene) with a defined molecular weight and a low polydispersity. *Macromolecules* **2004**, *37*, 1169–1171.
35 Sheina, E.; Liu, J.; Iovu, M. C.; Laird, D. W.; Mccullough, R. D. Chain growth mechanism for regioregular nickel-initiated cross-coupling polymerizations. *Macromolecules* **2004**, *37*, 3526–3528.
36 Verheyen, L.; Timmermans, B.; Koeckelberghs, G. Influence of the sequence in conjugated triblock copolymers on their aggregation behavior. *Macromolecules* **2018**, *51*, 6421–6429.
37 Pal, S.; Nandi, A. K. Cocrystallization behavior of poly(3-alkylthiophenes): influence of alkyl chain length and head to tail regioregularity. *Macromolecules* **2003**, *36*, 8426–8432.
38 Tai, Q.; Zhao, X.; Yan, F. Hybrid solar cells based on poly(3-hexylthiophene) and electrospun TiO_2 nanofibers with effective interface modification. *J. Mater. Chem.* **2010**, *20*, 7366–7371.

https://doi.org/10.1007/s10118-023-2916-4